Correlations between Optical, Chemical and Physical Properties of Biomass Burn Aerosols

R. J. Hopkins,[1] K. Lewis,[2] Y. Desyaterik,[3] Z. Wang,[1,4] A. V. Tivanski,[1] W. P. Arnott,[2] A. Laskin,[3] and M. K. Gilles[1,*]

[1]Chemical Sciences Division, Lawrence Berkeley National Laboratory, Berkeley, California, USA.

[2]Department of Physics, University of Nevada, Reno, Nevada, USA.

[3]William R. Wiley Environmental Molecular Sciences Laboratory, Pacific Northwest National Laboratory, Richland, Washington, USA.

[4]College of Engineering, University of California, Berkeley, California, USA.

Abstract

Aerosols generated from burning different plant fuels were characterized to determine relationships between chemical, optical and physical properties. Single scattering albedo (ω) and Angstrom absorption coefficients (α_{ap}) were measured using a photoacoustic technique combined with a reciprocal nephelometer. Carbon-to-oxygen atomic ratios, sp^2 hybridization, elemental composition and morphology of individual particles were measured using scanning transmission X-ray microscopy coupled with near-edge X-ray absorption fine structure spectroscopy (STXM/NEXAFS) and scanning electron microscopy with energy dispersion of X-rays (SEM/EDX). Particles were grouped into three categories based on sp^2 hybridization and chemical composition. Measured ω (0.4 – 1.0 at 405 nm) and α_{ap} (1.0 - 3.5) values displayed a fuel dependence. The category with sp^2 hybridization >80% had values of ω (<0.5) and α_{ap} (~1.25) characteristic of light absorbing soot. Other categories with lower sp^2 hybridization (20 to 60%) exhibited higher ω (>0.8) and α_{ap} (1.0 to 3.5) values, indicating increased absorption spectral selectivity.

1. Introduction

The atmospheric radiation budget is strongly coupled with aerosols produced during natural and anthropogenic biomass burns. Biomass burn aerosols consist of particulate organic carbon (OC), soot or black carbon (BC) and inorganic species [*Reid, et al.*, 2005]. BC is strongly light absorbing, while OC mostly scatters radiation. Hence, biomass burn aerosols both scatter and absorb light, directly affecting the atmospheric radiation budget. They also impact climate indirectly by serving as cloud condensation nuclei (thus altering cloud optical properties) and by providing a surface for condensation of secondary organic aerosols. To estimate their radiative contributions, a range of chemical and physical properties are needed, including particle chemical composition, size, shape and hygroscopicity. These properties depend on the type of biomass fuel, the combustion phase of the fire (flaming *versus* smoldering) and the degree of subsequent atmospheric processing. Laboratory burns of biomass fuels provide an opportunity to explore the fundamental relationships between the chemical, physical and optical properties of particles

In this letter, chemical, physical and optical properties are reported for the combustion products of twelve biomass fuels typical of western and south-eastern U.S. forests. Scanning transmission X-ray microscopy (STXM) coupled with near-edge X-ray absorption fine structure (NEXAFS) spectroscopy enables determination of percent sp^2 hybridization (graphitic nature) and carbon-to-oxygen atomic ratios (C/O). Computer controlled scanning electron microscopy with energy dispersion of X-rays (CCSEM/EDX) yields particle morphology and elemental composition. In addition, aerosol single scattering albedo (ω), which is the ratio of light scattering and extinction at a particular wavelength was measured at 405 and 532 nm. The Angstrom coefficient for absorption (α_{ap}) was determined between these wavelengths and 870 nm using eq. 1.

$$\alpha_{ap} = \frac{\ln\left(\frac{\beta_{ap}(\lambda)}{\beta_{ap}(870)}\right)}{\ln\left(\frac{870}{\lambda}\right)} \qquad (1)$$

Where λ is wavelength (405 nm or 532 nm) and β_{ap} (λ) is aerosol light absorption measured at specific λ. Hence, variations in optical properties can be correlated with the nature of the relevant chemical bonds.

2. Experiment

Experiments were conducted at the U.S. Forest Service Fire Science Laboratory (FSL, Missoula, MT), from July 5–9, 2006. Fuels in Table 1 were selected to represent mid-latitude forest burning [*Chakrabarty, et al.*, 2006]. Fuels (200 g) were placed upon a platform in an open room, ignited with a propane torch and went through a combination of flaming and smoldering phases for ~5-10 minutes. Hence, particulates collected during the hour after the fires extinguished contained matter from a mixture of combustion phases. Photographs taken during the burns were examined to determine if flaming and/or smoldering were observed as noted in Table 1. Particles were collected onto Si_3N_4 windows (Silson Ltd) and TEM grids (Carbon type B on Cu 400 mesh grids, Ted Pella Inc) for STXM and SEM analysis, respectively, using a rotating cascade impactor, MOUDI model 110 (MSP, Inc). Size-fractionated particles of 0.32-0.56 μm aerodynamic diameters, studied here were collected on the 7th stage MOUDI impactor stage.

STXM analysis was performed at beamline 5.3.2 of the Advanced Light Source (Berkeley, CA) [*Warwick, et al.*, 2002] at the carbon (C) (280–320 eV) and oxygen (O) (520–550 eV) absorption edges [*Hopkins, et al.*, 2007]. C/O atomic ratios are calculated using a method outlined previously [*Hopkins, et al.*, 2007; *Tivanski, et al.*, 2007]. For ease of visual comparison, spectra presented here are normalized to the same carbon concentration. CCSEM/EDX analysis was at the Environmental Molecular Sciences Laboratory (Richland, WA), using a FEG XL30 digital scanning electron microscope (FEI, Inc) equipped with an EDX spectrometer (EDAX, Inc). Specific details of the analysis are provided elsewhere [*Laskin, et al.*, 2006].

Light absorption and scattering measurements were obtained in-situ during the burns with a photoacoustic instrument [*Arnott, et al.*, 2005] modified to operate simultaneously at two wavelengths (405 and 870 nm). Light scattering was measured using the reciprocal nephelometer

method [*Abu-Rahmah, et al.*, 2006]. A second single wavelength instrument provided aerosol scattering and absorption measurements at 532 nm. Instrument calibration is performed by comparing extinction with scattering for very weakly absorbing salt aerosol, and also for strongly absorbing kerosene soot aerosol [*Abu-Rahmah, et al.*, 2006].

3. Results and Discussion

3.1 Chemical and Physical Characterization

Chemical and physical properties determined from CCSEM/EDX and STXM/NEXAFS suggest classification of the combustion products into three categories: 1) liquid/oily OC with BC inclusions, 2) mixed carbonaceous and inorganic material and 3) BC material with inorganic inclusions (see Table 1). Figure 1 presents a characteristic SEM image and EDX and NEXAFS spectra recorded from particulate matter for each category. The NEXAFS spectra were obtained by averaging over 10 μm × 10 μm regions containing multiple particles.

CCSEM/EDX elemental analysis (Figure 1(b)) suggests that category 1 materials are composed mainly of C and O with no inorganic inclusions. SEM images indicate that these products contain different types of particulate matter. The small carbonaceous particles resembling fragments of soot fractals surrounded by irregularly shaped oily regions containing C and O have been reported previously [*Buseck and Pósfai*, 1999; *Chen, et al.*, 2005; *Pósfai, et al.*, 2004]. The oily/tar-like residue may be produced by a heavy oil type of combustion, which is more typical in the absence of inorganic salts [*Jones, et al.*, 2007]. NEXAFS spectra indicate that the inclusions have a high 1s-π* aromatic carbon peak (R'–C=C–R") at 285.3 eV [*Hopkins, et al.*, 2007], consistent with the presence of soot. In addition, a high proportion of oxygen-containing functional groups are observed in the 286.8–289.7 eV region (highlighted in Figure 1). This indicates that graphitic material is not the dominant species as it displays a low proportion of oxygen-containing functional groups relative to R'–C=C–R". C/O atomic ratios range from 69/31–87/13, with a mean value of 78/22 (see Table 1).

Category 2 combustion products are carbonaceous material mixed with inorganic species. The SEM/EDX spectrum in Figure 1(e) indicates prominent K and Cl peaks and lower C and O compared to categories 1 and 3. Normalizing the NEXAFS spectra in Figures 1(c, f, i) to the

same carbon concentration required multiplying category 2 spectra by ~2; category 2 materials are less carbonaceous than categories 1 and 3. Combustion products in category 2 display C/O ratios ranging from 74/26–77/23, with a mean value of 76/24.

SEM images and NEXAFS spectra indicate that despite similar SEM/EDX spectra, category 1 and 3 materials display significant morphological and chemical bonding differences. Category 3 materials have a fractal morphology, typical of soot (Figure 1(g)) e.g. [*Buseck and Pósfai*, 1999; *Chen, et al.*, 2005; *Pósfai, et al.*, 2004]. Figure 1(i) illustrates striking similarities between NEXAFS spectra from a category 3 material and flame generated methane soot defined as 100% BC [*Kirchstetter and Novakov*, 2007]. Similarities include intense 1s-π* R'–C=C–R" (285.3 eV) and 1s-σ* R'–C=C–R" (292.3 eV) peaks, and the lower intensity 286.8–289.7 eV region, where oxygen-containing functional group peaks are typically observed. The C/O ratio for methane soot is 84/16, which is within the C/O ratio range of 80/20–91/9 displayed by category 3 materials.

3.2 Optical Properties

Correlating optical properties ω and α_{ap} with chemical and physical information enables an understanding of the variation in light absorption of these biomass burn particles. The percent sp^2 hybridization is calculated from the NEXAFS spectra [*Hopkins, et al.*, 2007]. This value reflects the graphitic nature of a material, with 100% sp^2 hybridization corresponding to highly oriented pyrolytic graphite. In our previous work, the 282-292 eV spectral region was fit using a series of Gaussian functions and the sp^2 hybridization estimated [*Hopkins, et al.*, 2007]. Here, only the 1s-π* R'–C=C–R" peak (~285 eV) is fit, providing an upper limit for the sp^2 hybridization value. Category 1, 2 and 3 combustion products exhibit sp^2 hybridization values between 25–44% (mean 34%), 48–60% (mean 53%) and 81–86% (mean 83%), respectively (see Table 1). The sp^2 hybridization and C/O ratio of methane soot is similar to that of category 3 fuels indicating a similarity in optical properties and chemical bonding.

Figure 2 illustrates the relationship between ω measured at both 405 and 532 nm (grey and black symbols, respectively) and percent of sp^2 hybridization for the various combustion particulates. As the percent of sp^2 hybridization increases, a decrease in ω at both wavelengths is

observed. Mean ω values of 0.895, 0.879 and 0.409 at 405 nm and 0.939, 0.838 and 0.394 at 532 nm were measured for categories 1, 2 and 3, respectively. These illustrate the relatively non-absorbing nature of category 1 and 2 particulate matter (low BC relative to OC plus inorganic material) and the greater light absorbing capabilities of category 3 particulates (high proportion of BC).

Despite the similarity in percent sp^2 hybridization values of category 3 materials and methane soot, their ω values are different. Methane soot has a ω of 0.15 at 530 [*Kirchstetter and Novakov*, 2007]. The decreased absorption of category 3 materials may arise from perturbation of the extended π networks by the presence of inorganic inclusions not found in laboratory generated methane soot. This disparity could arise if the methane soot particles were smaller than those from biomass combustion.

In Figure 3, α_{ap} values range from 0.9–3.4 at 405 nm and 0.9–2.3 at 532 nm, indicating a clear difference in the spectral dependence for the biomass combustion particulates. Generally, α_{ap} increases as percent sp^2 hybridization decreases, thus category 1 and 2 materials display a strong spectral dependence, typical of organic aerosols [*Kirchstetter, et al.*, 2004]. Previous work indicates that biomass burning smoke varies more strongly with wavelength than urban and soot aerosols [*Bergstrom, et al.*, 2003; *Bergstrom, et al.*, 2002; *Dubovik, et al.*, 1998; *Horvath*, 1997; *Kirchstetter, et al.*, 2004; *Patterson and McMahon*, 1984; *Rosen, et al.*, 1978]. The stronger spectral dependence of biomass burn aerosols results from enhanced absorption at wavelengths <600 nm. Category 3 materials display low mean α_{ap} values, 1.13 and 1.11 at 405 and 532 nm, respectively, signifying a weak spectral dependence. Combustion particulate products with sp^2 hybridization values >80% display lower ω and α_{ap} values, indicating the highly absorbing nature of these graphitic materials.

4. Conclusions

Particles collected during combustion of biomass fuels are examined using microspectroscopy techniques, providing information on their chemical and physical properties. Subsequent assignment of the combustion particulate products into three categories based on

their morphology, elemental composition, chemical bonding, C/O ratios and percent sp^2 hybridization was made. The particulates comprising these three categories display diverse chemical and physical properties. ω and α_{ap} values measured *in situ* during the combustion process display a wide range of values (0.364–0.996 and 0.9–3.4, respectively), demonstrating the diversity in optical properties of biomass burning products. Only a single category, that comprises 25% of the combustion products is similar to BC, displaying high sp^2 hybridization and ω and α_{ap} values that indicate high light absorption ability.

It is generally accepted that flaming conditions produce more BC and less OC while smoldering fires result in higher OC content [*Ward, et al.*, 1992]. This is consistent with the strong flaming noted and the sp^2 hybridization and optical properties measured for category 3 fuels. However, several category 2 fuels exhibited a strong flaming phase and produced significant salts during the burning process, resulting in less carbonaceous particulate matter and optical properties inconsistent with BC. Category 1 fuels exhibited a range of burning conditions, including flaming, yet produced particulates more characteristic of OC with the corresponding optical properties. Hence, it appears that even when a flaming phase occurs, high salt contents and/or other fuel properties may influence the chemical and optical properties of particulate matter produced.

Acknowledgements

This work was supported by the Atmospheric Science Program of the U.S. Department of Energy, office of Biological and Environmental Research (OBER). The ALS is supported by the Director, Office of Science, Office of Basic Energy Sciences, Division of Chemical Sciences, Geosciences, and Biosciences of the U.S. Department of Energy at Lawrence Berkeley National Laboratory under Contract No. DE-AC02-05CH11231. The CCSEM/EDX analysis was performed in the Environmental Molecular Sciences Laboratory, a DOE OBER sponsored national scientific user facility located at the Pacific Northwest National Laboratory and operated for DOE by Battelle Memorial Institute under contract DE-AC06-76RL0. The authors gratefully acknowledge W. Malm and W. M. Hao for organizing the FLAME project which was funded by the Joint Fire Science Program and A. L. D. Kilcoyne for providing assistance at beamline 5.3.2.

We thank the staff of the USDA/USFS Fire Sciences Laboratory for their assistance with the studies.

References

Abu-Rahmah, A., W. P. Arnott and H. Moosmüller (2006), Integrating nephelometer with a low truncation angle and an extended calibration scheme, *Meas. Sci, Technol.*, *17*, 1723-1732.

Arnott, W. P., B. Zielinska, C. F. Rogers, J. Sagebiel, K. H. Park, J. Chow, H. Moosmüller, J. G. Watson, K. Kelly, D. Wagner, A. Sarofim, J. Lighty and G. Palmer (2005), Evaluation of 1047-nm photoacoustic instruments and photoelectric aerosol sensors in source-sampling of black carbon aerosol and particle-bound PAHs from gasoline and diesel powered vehicles, *Environ. Sci., Technol.*, *39*, 5398-5406.

Bergstrom, R. W., P. Pilewskie, B. Schmid and P. B. Russell (2003), Estimates of the spectral aerosol single scattering albedo and aerosol radiative effects during SAFARI 2000, *J. Geophys. Res. Atmos. 108*, doi:10.1029/2002JD002435.

Bergstrom, R. W., P. B. Russell and P. Hignett (2002), Wavelength dependence of the absorption of black carbon particles: Predictions and results from the TARFOX experiment and implications for the aerosol single scattering albedo, *J. Atmos. Sci.*, *59*, 567-577.

Buseck, P. R. and M. Pósfai (1999), Airborne minerals and related aerosol particles: Effects on climate and the environment, *Proceedings of the National Academy of Sciences*, *96*, 3372-3379.

Chakrabarty, R. K., H. Moosmüller, M. A. Garro, W. P. Arnott, J. Walker, R. A. Susott, R. E. Babbitt, C. E. Wold, E. N. Lincoln and W. M. Hao (2006), Emission from the laboratory combustion of wildland fuels: Particle morphology and size, *J. Geophys Res. Atmos. 111*, doi:10.1029/2005JD006659.

Chen, Y., N. Shah, A. Braun, F. E. Huggins and G. P. Huffman (2005), Electron microscopy investigation of carbonaceous particulate matter generated by combustion of fossil fuels, *Energy & Fuels*, *19*, 1644-1651.

Christian, T. J., B. Kleiss, R. J. Yokelson, R. Holzinger, P. J. Crutzen, W. M. Hao, B. H. Saharjo and D. E. Ward (2003), Comprehensive laboratory measurements of biomass-burning emissions: 1. Emissions from Indonesian, African, and other fuels, *J. Geophys. Res. Atmos. 108*, doi:10.1029/2003JD003704.

Dubovik, O., B. N. Holben, Y. J. Kaufman, M. Yamasoe, A. Smirnov, D. Tanré and I. Slutsker (1998), Single-scattering albedo of smoke retrieved from the sky radiance and solar transmittance measured from ground, *J. Geophy. Res. 103*, 31,903-31,923.

Henke, B. L., P. Lee, T. J. Tanaka, R. L. Shimabukuro and B. K. Fuikawa (1982), Low-energy X-ray interaction coefficients: Photoabsorption, scattering, and reflection : E = 100-2000 eV Z = 1-94, *Atomic Data and Nuclear Data Tables*, *27*, 1-144.

Hopkins, R. J., A. V. Tivanski, B. D. Marten and M. K. Gilles (2007), Chemical bonding and structure of black carbon reference materials and individual carbonaceous atmospheric aerosols, *J. Aeros. Sci.*, *38,* 573-591.

Horvath, H. (1997), Experimental calibration for aerosol light absorption measurements using the integrated plate method-Summary of the data, *J. Aeros. Sci.*, *28*, 1149-1161.

Jones, J. M., L. I. Darvell, T. G. Bridgeman, M. Pourkashanian and A. Williams (2007), An investigation of the thermal and catalytic behaviour of potassium in biomass combustion, *Proceedings of the Combustion Institute*, *31*, 1955-1963.

Kirchstetter, T. W. and T. Novakov (2007), Controlled generation of black carbon particles from a diffusion flame and applications in evaluating BC measurement methods, *Atmos. Environ.*, *41*, 1874-1888.

Kirchstetter, T. W., T. Novakov and P. V. Hobbs (2004), Evidence that the spectral dependence of light absorption by aerosols is affected by organic carbon, *J. Geophys. Res. Atmos. 109*, doi:10.1029/2004JD004999.

Laskin, A., J. P. Cowin and M. J. Iedema (2006), Analysis of individual environmental particles using modern methods of electron microscopy and X-ray microanalysis, *J. Elec. Spectros. Rel. Phenom.*, *150*, 260-274.

Patterson, E. M. and C. K. McMahon (1984), Absorption characteristics of forest fire particulate matter, *Atmos. Environ.*, *18*, 2541-2551.

Pósfai, M., A. Gelencser, R. Simonics, K. Arato, J. Li, P. V. Hobbs and P. R. Buseck (2004), Atmospheric tar balls: Particles from biomass and biofuel burning, *J. Geophys. Res. Atmos.*, *109*, D06213, doi:06210.01029/02003JD004169.

Reid, J. S., R. Koppmann, T. F. Eck and D. P. Eleuterio (2005), A review of biomass burning emissions part II: intensive physical properties of biomass burning particles, *Atmos. Chem. Phys. 5*, 799-825.

Rosen, H., A. D. A. Hansen, L. Gundel and T. Novakov (1978), Identification of the optically absorbing component in urban aerosol, *Appl. Opt.*, *17*, 3859-3861.

Tivanski, A. V., R. J. Hopkins and M. K. Gilles (2007), Oxygenated interface on biomass burn tar balls determined by single particle scanning transmission X-ray microscopy, *J. Phys. Chem. A., 111*, 5448-5458.

Ward, D. E., R. A. Susott, J. B. Kauffman, R. E. Babbitt, D. L. Cummings, B. Dias, B. N. Holben, Y. J. Kaufman, R. A. Rasmussen, and A. W. Setzer (1992), Smoke and Fire Characteristics for Cerrado and Deforestation Burns in Brazil: BASE-B Experiment, *J. Geophys. Res.*, *97D, 14601-14619.*.

Warwick, T., H. Ade, D. Kilcoyne, M. Kritscher, T. Tylisczcak, S. Fakra, A. Hitchcock, P. Hitchcock & H. Padmore (2002), A new bend-magnet beamline for scanning transmission X-ray microscopy at the Advanced Light Source, *J. Sync. Rad.*, *9*, 254-257.

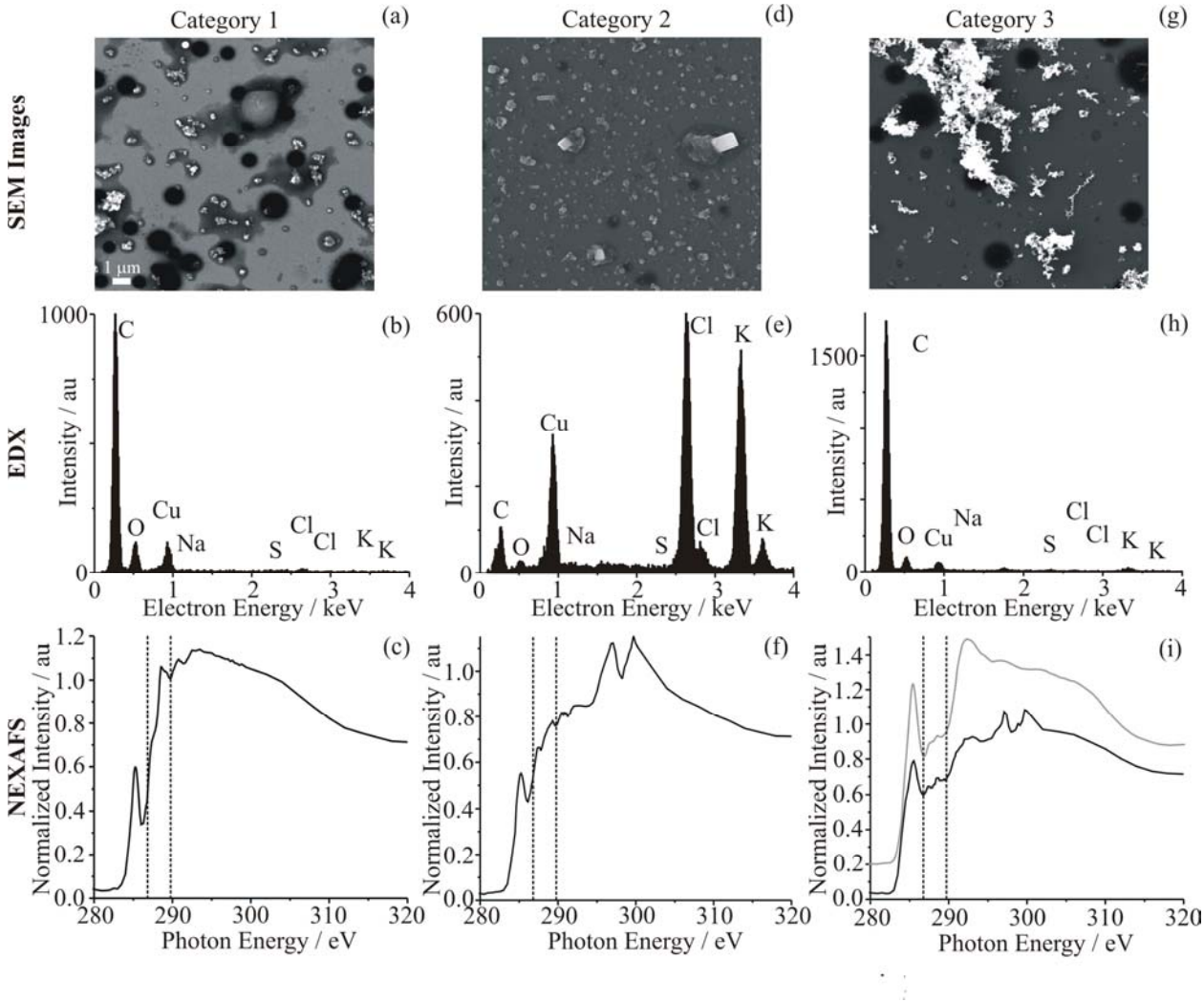

Figure 1 Characteristic SEM images, EDX and NEXAFS spectra of three types of particulates generated from the burning of (a-c) Ponderosa pine needles and sticks, (d-f) rice straw and (g-i) Chamise. The grey NEXAFS spectrum presented in (i) was recorded from methane soot and is shown for comparison purposes. Dotted lines on the NEXAFS spectra indicate the 286.8–289.7 eV region where oxygenated functional groups are typically located. The doublet peak near 300 eV arises from K [*Henke, et al.*, 1982]. Dark round spots in the SEM micrographs are surface features of the substrate carbon film.

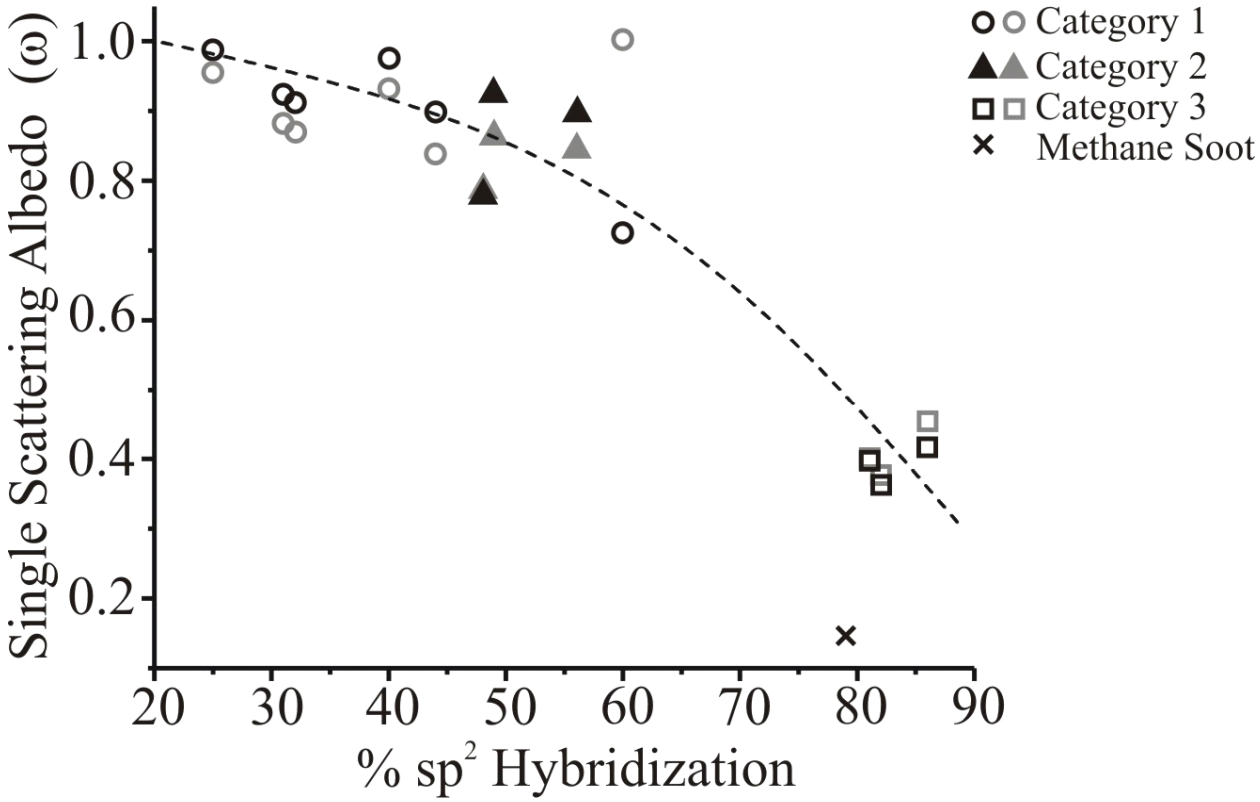

Figure 2 Relationship between single scattering albedo (ω) and percent of sp^2 hybridization for the twelve biomass fuels and methane soot. Black and grey symbols represent ω recorded at 532 and 405 nm, respectively. The dashed line serves as a visual guide.

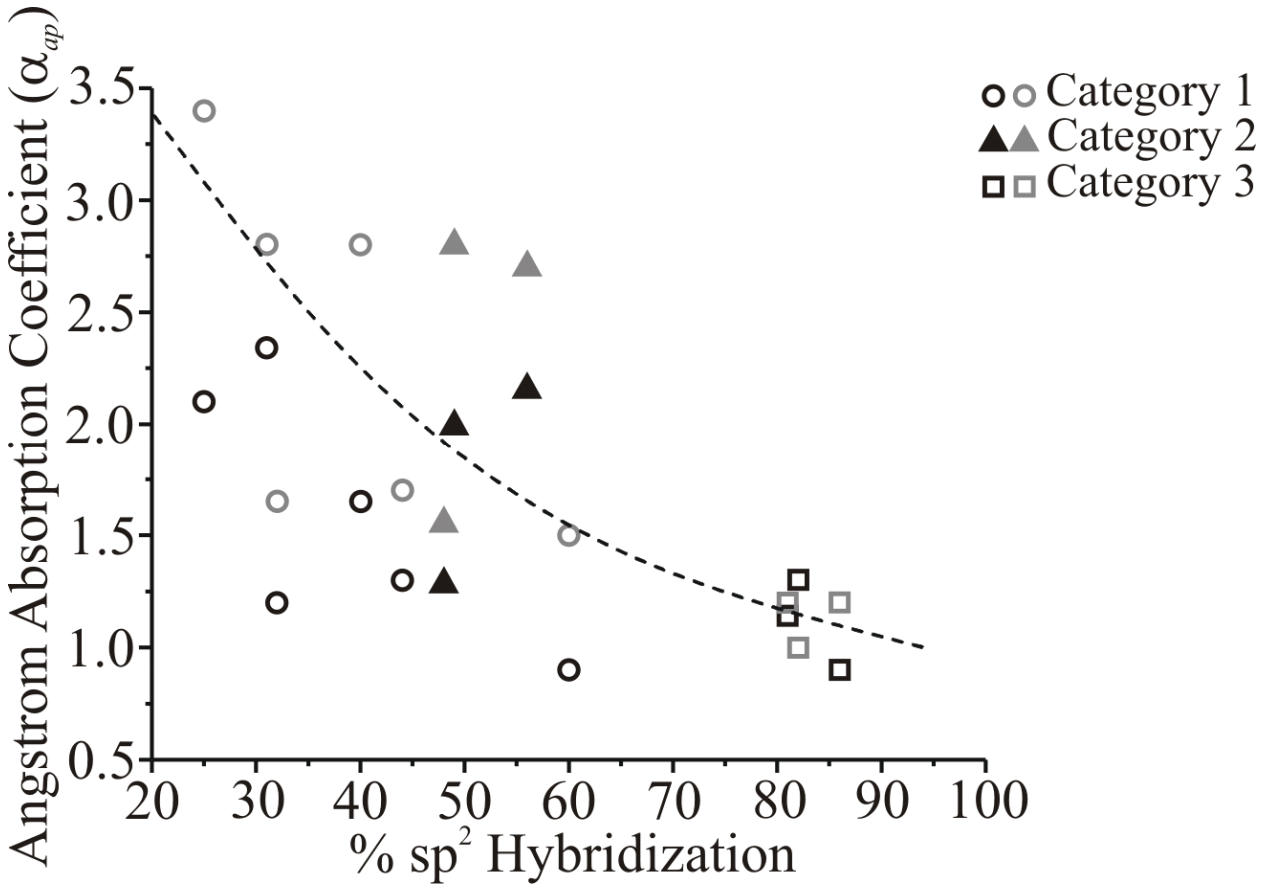

Figure 3 Relationship between Angstrom absorption coefficient (α_{ap}) and percent of sp^2 hybridization for the biomass fuels. Black and grey symbols represent α_{ap} recorded at 532 and 405 nm, respectively. The dashed line serves as a visual guide.

Table 1. Biomass burning particulates classified according to chemical and physical properties determined by CCSEM/EDX and STXM/NEXAFS.

Category 1 [a]	**C/O**	**%sp^2**	**Flaming**	**Smoldering**
Ponderosa Pine (Needles & Twigs)	70/30	32	Yes	Yes
Ponderosa Pine (Duff)	87/13	40	No	Yes (s)[b]
Alaskan Tundra Core (Duff)	82/18	25	No	Yes (s)
Southern Longleaf Pine Needles	69/31	44	Yes (s)	Yes
Puerto Rico Mixed Woods	80/20	60	Yes	Yes
Ceanothus (I)[c]	78/22	31	Yes	Yes
	Mean 78/22	**Mean 39**		
Category 2				
Rice Straw (I)		49	Yes (s)	-[d]
Puerto Rico Maiden Fern (dried) (I)	74/26	56	Yes	-
Palmetto (I)	77/23	48	Yes (s)	-
	Mean 76/24	**Mean 51**		
Category 3				
Chamise (I)	80/20	81	Yes (s)	Yes
Juniper Foliage & Twigs (I)	91/9	82	Yes (s)	Yes
Sagebrush & Rabbitbush (I)	84/16	86	Yes (s)	-
	Mean 85/15	**Mean 83**		
Soot Standard				
Methane Soot	84/16	79		

[a] Species: Pinus ponderosa; Pinus palustris; Tectona grandis, Hibiscus tilliaceus L., Peltophorum inerme, Inga laurina; Ceanothus crassifolius; Oryza L.; Thelypteris yaucoensis; Serenoa repens; Adenostoma fasciculatum; Juniperus osterosperma; Artemisia tridentate, Ericameria nauseosa.

[b] s (strong) indicates that the flame height was greater than twice the burn pile width.

[c] (I) indicates the presence of inorganic material (including Na, Cl and K).

[d] A dash (-) indicates that a clear assessment could not be made.